

Are mergers responsible for universal halo properties?

Jie Wang^{*}, Simon D. M. White[†]

Max-Planck-Institut für Astrophysik, Karl-Schwarzschild-Str. 1, D-85748 Garching, Germany

Accepted 2008 ???? ?. Received 2008 ???? ?; in original form 2008 ???? ?

ABSTRACT

N -body simulations of Cold Dark Matter (CDM) have shown that, in this hierarchical structure formation model, dark matter halo properties, such as the density profile, the phase-space density profile, the distribution of axial ratio, the distribution of spin parameter, and the distribution of internal specific angular momentum follow ‘universal’ laws or distributions. Here we study the properties of the first generation of haloes in a Hot Dark Matter (HDM) dominated universe, as an example of halo formation through monolithic collapse. We find all these universalities to be present in this case also. Halo density profiles are very well fit by the Navarro et al (1997) profile over two orders of magnitude in mass. The concentration parameter depends on mass as $c \propto M^{0.2}$, reversing the dependence found in a hierarchical CDM universe. However, the concentration-formation time relation is similar in the two cases: earlier forming haloes tend to be more concentrated than their later forming counterparts. Halo formation histories are also characterized by two phases in the HDM case: an early phase of rapid accretion followed by slower growth. Furthermore, there is no significant difference between the HDM and CDM cases concerning the statistics of other halo properties: the phase-space density profile; the velocity anisotropy profile; the distribution of shape parameters; the distribution of spin parameter, and the distribution of internal specific angular momentum are all similar in the two cases. Only substructure content differs dramatically. These results indicate that mergers do not play a pivotal role in establishing the universalities, thus contradicting models which explain them as consequences of mergers.

Key words: neutrinos—methods:N-body simulations – methods: numerical—dark matter

1 INTRODUCTION

The mass distribution of the self-gravitating, quasi-equilibrium dark haloes that form in an expanding universe is an issue of fundamental importance. Early work on self-similar spherical collapse predicts virialized structures with power-law density profiles (Fillmore & Goldreich 1984; Bertschinger 1985). As N -body techniques improved, it was realised that, in the hierarchical universes, the profile departs significantly from a single power law and is better fitted by a profile with curvature in a log-log plot. (Efstathiou et al. 1985; Dubinski & Carlberg 1991). Later, it was established that the density profiles of haloes in CDM and other hierarchical clustering cosmologies, have a universal form which is well represented by the simple fitting formula of Navarro et al. (1996, 1997, hereafter NFW)

$$\rho(r) = \frac{\rho_s}{(r/r_s)(1+r/r_s)^2} \quad (1)$$

where r_s is a characteristic radius where the logarithmic density slope is -2 , and $\rho_s/4$ is the density at r_s . The above equation implies that $\rho \propto r^{-1}$ in the inner regions and $\rho \propto r^{-3}$ in the outskirts. A useful alternative parameter for describing the shape of the profile is the concentration parameter $c = r_{200}/r_s$ (r_{200} is the virial radius defined as the radius within which the mean density is 200 times the critical value). Shortly after the NFW papers, Huss et al. (1999b) showed that the NFW model also fit halos which form by monolithic collapse (i.e. without mergers) in a HDM cosmology. Nevertheless much work has focused on the role of mergers in establishing the NFW profile, since mergers contribute substantially to the growth of haloes in the CDM model (Raig et al. 1998; Salvador-Sole et al. 1998; Syer & White 1998; Subramanian et al. 2000; Dekel et al. 2003). Syer & White (1998) analysed dynamical processes during repeated mergers, concluding that the universal profile is generated by tidal stripping of small haloes as they merge into larger objects. Dekel et al. (2003) extended this model and found the tidal compression from a halo core makes the satellite orbits decay from the radius where $\rho \propto r$

* Email: wangjie@mpa-garching.mpg.de

† Email: swhite@mpa-garching.mpg.de

to the halo center and causes a rapid steepening of the inner profile to $\rho \propto r^{-\alpha}$ ($\alpha > 1$). Recent work has confirmed the NFW hypothesis, extending the comparison to a much wider range of densities and radii than the original work, and uncovering small but significant deviation, between the mean density profiles of simulated dark halos and the NFW formula (Power et al. 2003; Diemand et al. 2004; Merritt et al. 2006; Graham et al. 2006; Gao et al. 2008; Hayashi & White 2007). The differences, however, are quite small compared to the scatter between different haloes of the same mass.

In addition to the density profile, other halo properties are found to follow universal profiles or universal distributions in the hierarchical CDM model. The “phase-space density” $\rho(r)/\sigma^2(r)$ has a remarkably accurate pure power-law distribution with radius (Taylor & Navarro 2001; Barnes et al. 2006). The distributions of shape parameters (e.g. the axis ratios) have a weak dependence on mass and redshift (Bullock 2002; Kasun & Evrard 2005; Allgood et al. 2006; Bett et al. 2007). The spin parameter distribution is well described by a log-normal function which varies weakly with halo mass (Barnes & Efstathiou 1987; Warren et al. 1992; Cole & Lacey 1996; Bullock et al. 2002; Bett et al. 2007). Bullock et al. (2001) also found that the cumulative mass distribution of specific angular momentum j is well fitted by a universal function. All these distributions appear to depend little, if at all, on the global cosmological parameters and on the shape of the initial matter power spectrum. However, the origin of these universalities is still not well understood.

In this paper, we will test whether mergers are the dominant physical mechanism to produce these universal profiles or distributions. To this end, we study a range of properties of the haloes which grow by two different paradigms, by hierarchical aggregation and monolithic collapse. The concordance cosmology (Λ CDM) is a standard hierarchical universe, and the HDM dominated universe provides an example where formation of the first haloes is monolithic. In a HDM universe, small objects cannot form because free-streaming effects smooth out small-scale structure in the initial condition. The first halos then form by smooth collapse.

We begin in section 2 with a summary of the N -body simulations and halo catalogues used in this paper. In section 3, we give a general description of how halos form and evolve in the HDM universe. In section 4, a range of halo properties are studied in depth in our two model universes. Then, we will summarise and discuss our results in section 5.

2 THE SIMULATIONS AND HALO CATALOGUES

In this work, we simulate the HDM density field using 512^3 particles within a $100h^{-1}$ Mpc cube. For simplicity, we choose an Einstein-de Sitter universe dominated by a single massive neutrino. Then the cosmological matter density parameter is $\Omega_m = 1$ and the simulation particle mass is $2.07 \times 10^9 M_\odot/h$. The initial power spectrum used to perturb the initial particle set is based on the theoretical prediction of Bond & Szalay (1983). The power spectrum in a HDM universe possesses a coherent free streaming scale:

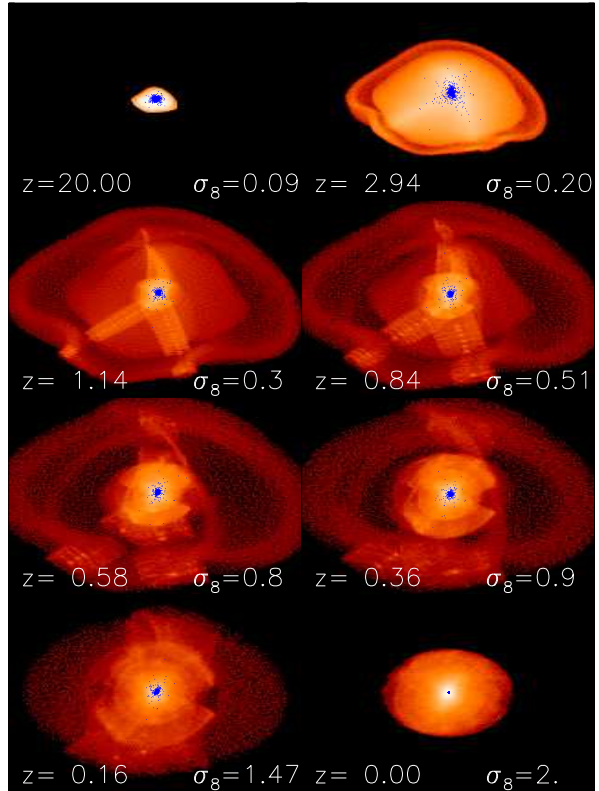


Figure 1. The evolution of a massive halo in a HDM universe with mass $1.3 \times 10^{15} M_\odot/h$ at redshift zero. All particles within r_{200} at $z = 0$ are traced back to seven higher redshifts. In addition the particles in the very inner region $r < 0.01r_{200}$ are traced back and are shown as the blue points. The size of each box is $8\text{Mpc}/h$ in physical (not comoving) units. The redshift and the corresponding σ_8 are showed in each panel.

$\delta_{\text{nu}} = 22.2\text{Mpc}$ in our case. The corresponding damping mass is $7.28 \times 10^{14} M_\odot/h$. This power spectrum is normalised to $\sigma_8 = 2$ which corresponds to the collapse of the first non-linear structures at $z \sim 6$. This simulation was presented as glass512 in Wang & White (2007, hereafter paper I) and more technical details can be found there. We choose to compare it with a simulation of the WMAP1 model from Wang et al. (2008). This simulates a concordance Λ CDM universe with 540^3 particles in a $125h^{-1}$ Mpc cube. Hereafter we refer these two simulations as HDMRUN and CDMRUN. The softening lengths for these two simulations are 10 and $5\text{kpc}/h$ in the HDM and CDM cases respectively.

As pointed out in Paper I, the population of haloes in HDMRUN is contaminated because discreteness effects break up the filaments and produce many artificial small haloes. The resolution limit above which haloes are immune to this effect is $M_{\text{lim}} = 8.8 \times 10^{12} M_\odot/h$, and corresponds to about 5000 particles. In the current study we therefore focus primarily on well resolved haloes with particle number $N_{200} > 10000$ within virial radius r_{200} in two simulations. Several of our most massive HDM haloes experience one or two major mergers at low redshift as in the CDM case.

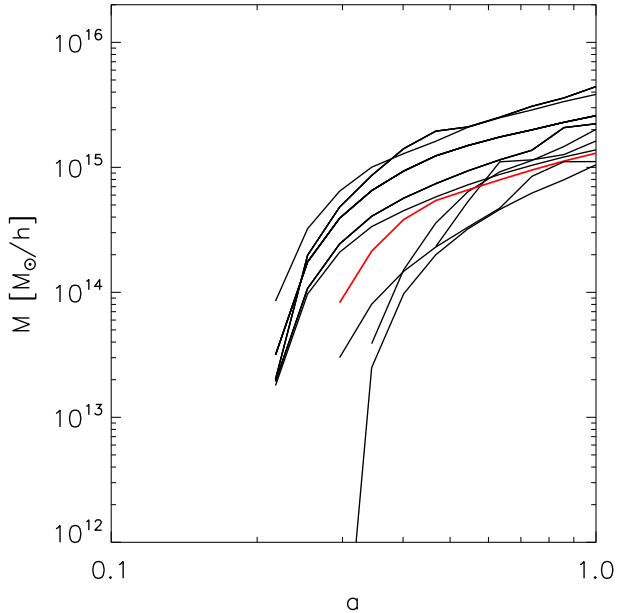


Figure 2. Mass assembly histories (MAH) for the 10 most massive haloes at $z = 0$ in the HDMRUN sample. The red curve indicates the halo presented in Fig. 1

We exclude these second generation haloes from our analysis below. The number of haloes which satisfy the above constraints is 58 and 304 in HDMRUN and CDMRUN respectively. When studying the M_{200} - c relation, we reduce the particle number limit to 5000 in order to cover a wider mass range. We then have 84 (HDMRUN) and 1752 (CDMRUN) haloes in the two simulations.

Our haloes are identified by a standard $b = 0.2$ friends-of-friends (FOF) group-finder (Davis et al. 1985). Then the SUBFIND algorithm (Springel et al. 2001) is used to resolve these objects into substructures and main subhaloes. The latter then define our halo sample through our N_{200} limits. At high redshift, the FOF method tends to link more particles together especially in our HDMRUN where large filaments and sheets are easily joined. SUBFIND defines the centre as the minimum of the gravitational potential, and this is used to estimate N_{200} . We also use merger trees built up from the subhalo catalogue produced by the SUBFIND algorithm (see Springel et al. 2005).

3 MONOLITHIC GROWTH

In Fig. 1, we study the evolution of a typical halo in our HDMRUN simulation. The mass of this halo is about twice the free-streaming mass scale. In the lower right corner ($z = 0$), all particles within r_{200} are chosen. These are then traced back to the initial condition in the other panels. The particles within the central region $r < 0.01r_{200}$ are also traced back to high redshift and are highlighted with blue points. It is interesting that these images are not similar to those found in the concordance CDM universe using a similar representation by Gao et al. (2004): the whole density

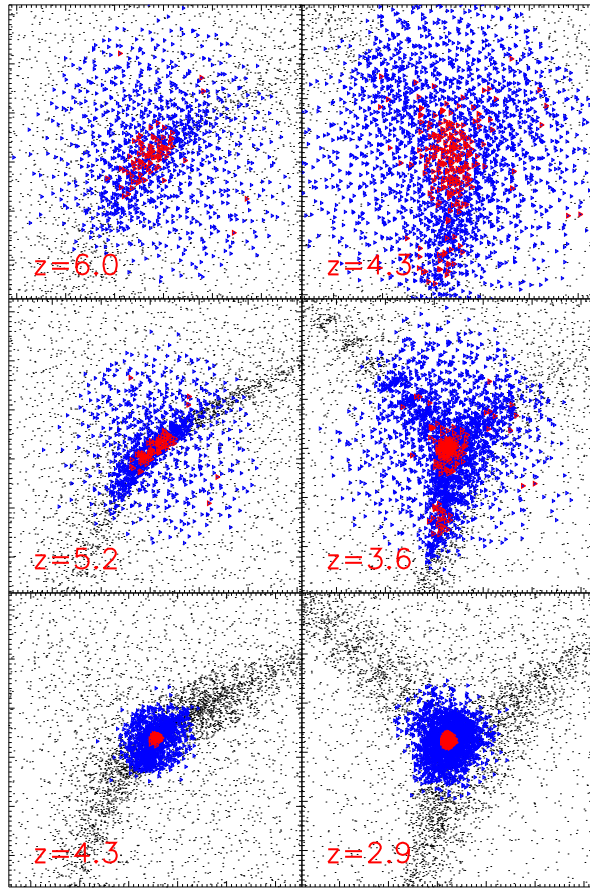


Figure 3. Formation histories of two “first” objects in a HDM universe. The right column shows a halo with $N_{200} = 2686$ at $z = 2.9$ (roughly $M_{200} = 3.5 \times 10^{14} M_{\odot}$); while the left column shows another halo with $N_{200} = 1215$ ($M_{200} = 1.6 \times 10^{14} M_{\odot}$) at $z = 4.3$. All particles in both halos at the last redshift are traced back to higher redshifts and presented as blue points. Particles in the very inner region $r < 0.1r_{200}$ are traced back and presented as red points. Other background particles are shown with black points. The coordinate is comoving scale, and the size of each box is 6Mpc/h. The redshift is labeled in each panel. The simulation glass128 (see Paper I) is used here. Note the artificial discreteness features visible in the filaments in the $z = 3.6$ panel.

field is smooth at all times and no obvious substructures are seen. The collapse along the filaments into knots occurs simultaneously with the accretion of diffuse particles. At redshift 1.14 and 0.84, some parts of the filaments are missing since they fall outside r_{200} at $z = 0$. The particles which end up within $0.01r_{200}$ stayed close together at all times, even in the initial condition. They fall to the centre in a smooth spherical collapse. In a CDM universe, as presented in Fig. 2. of Gao et al. (2004), the matter which ends up in the central region typically comes from a number of different objects at early times.

In Fig 2 we present the mass assembly history (MAH) of the 10 most massive haloes in the HDMRUN sample. This is just the mass growth of the most massive progenitor in each

case. We find that the MAHs are similar to those of haloes in a CDM universe: at early stages, the mass grows rapidly; but this slows dramatically towards $z = 0$. For example, the MAH of the halo shown in Fig. 1 is presented as a red curve in Fig 2. This halo stays in the rapid growth phase until $z = 1.2$, and its assembly is dominated by smooth spherical infall as Fig. 1 indicates. This appears quite different from the hierarchical growth described by Wechsler et al. (2002) and Zhao et al. (2003): their rapid growth phase is dominated by mergers. They also speculated that the universal inner density profile results from violent relaxation during this fast merger phase. We will see below that the density profile is also universal in our HDM simulation. Thus the NFW profile apparently does not require mergers, as noted originally by Huss et al. (1999a).

Halo formation histories obviously differ in CDM and HDM universes. Another interesting question is how and where the first objects form in the HDM case. Here we must keep in mind that the free-streaming scale in HDM is just a characteristic scale and its relationship to the actual mass of the first objects is not obvious. In Fig. 3, we present formation histories for two “first” objects. They were identified at $z = 4.3$ (left column) and $z = 2.9$ (right column) when they had gathered 1215 and 2686 particles within r_{200} respectively. In order to see the particles better, we here use a lower mass resolution simulation glass128 which was also presented in Paper I. This simulation has the same initial density field as HDMRUN, but 16 times lower mass resolution. As in Fig 1, we trace back all particles within r_{200} (blue) and within $0.1r_{200}$ (red) to higher redshift. Other background particles are shown as black points. It is obvious that both haloes form by smooth spherical collapse. In other words, the particles in the filaments and “voids” fall into the halo together. Even the particles within the central region ($< 0.1r_{200}$) seem to follow a roughly spherical collapse. This agrees with what we see in Fig 1. In the right column, the halo forms in a node which connects three filaments, and the halo forms almost at the same time as the three neighbour filaments. For the case in the left column, the halo forms at the end of one filament ($z = 6.0$) and then grows at the same time as another filament. We have also checked some other examples and find that almost all of them are born in nodes or at the ends of filaments and grow by spherical accretion.

Merger events in such a monolithic universe are expected to be rare. We find this to be true in our HDM simulations. For example, in HDMRUN, if we define merger events as the merging of ‘real’ haloes whose masses are larger than the mass limit, only a few haloes experience a major merger event (with mass ratio of the two progenitors greater than 1 : 3). We exclude these haloes from our study in this paper. Only about 30 percent of the remaining haloes experience minor merger events, and it is thus reasonable to regard them as a sample of ‘first’ haloes.

4 HALO PROPERTIES IN THE TWO UNIVERSES

In this section, we will study a range of “first” halo properties in the HDM universe and compare them with their counterparts in the Λ CDM model.

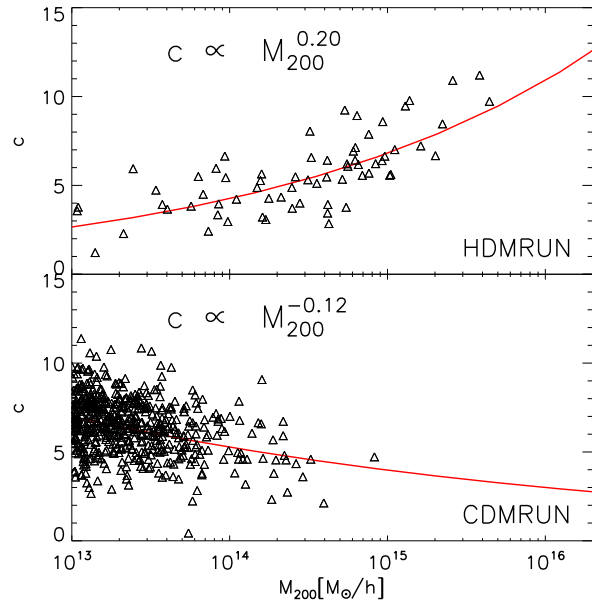


Figure 5. The distributions of halo mass M_{200} and concentration parameter c . The top panel is from HDMRUN and the bottom one from CDMRUN.

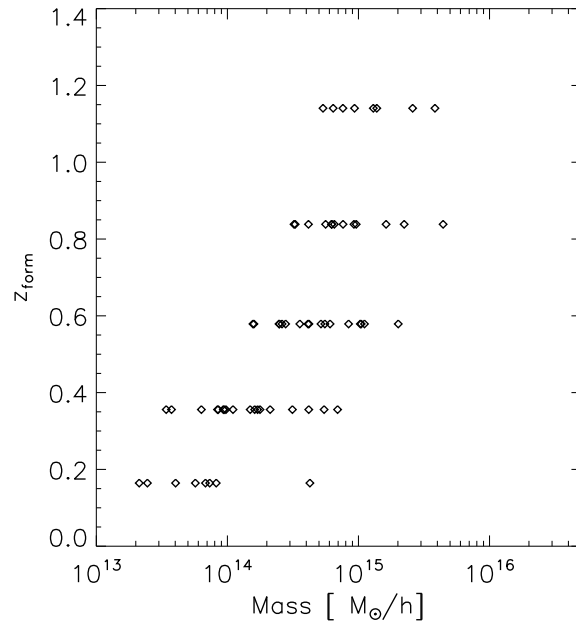


Figure 6. The distribution of formation time for haloes with $M_{200} \geq 10^{13} M_{\odot}/h$ in the HDMRUN sample.

4.1 Density Profile and Formation History

Previous studies (Moore et al. 1999; Colín et al. 2000; Eke et al. 2001; Busha et al. 2007) have focused on the formation of the first haloes in a WDM cosmology and have claimed that the density profiles of these haloes do not differ substantially from the NFW form found in a CDM universe. We support these findings also in our HDM case, con-

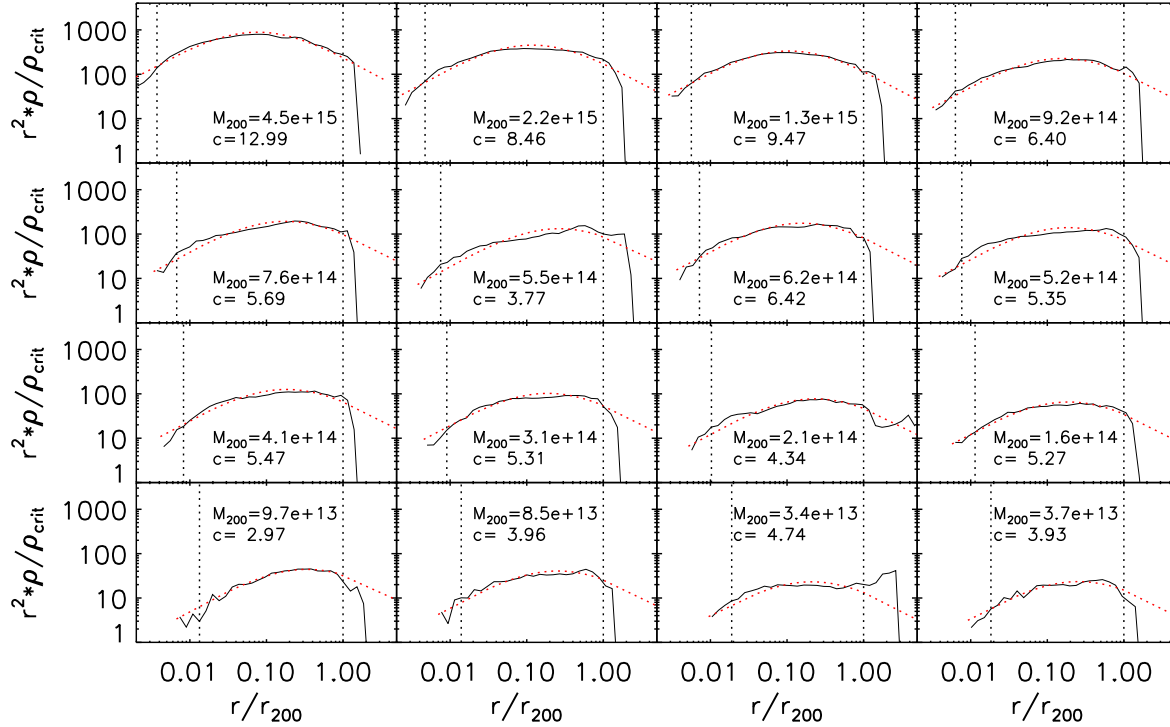


Figure 4. Density profiles for 16 haloes with particle number within r_{200} (N_{200}) greater than 10,000. These 16 haloes cover two orders of magnitude in mass. The density profiles are normalized by r^2/ρ_{crit} and the radius are normalized by r_{200} . In each panel, the red dotted curve is the NFW fit to the numerical measurement (black solid curve). Two vertical dotted lines show the softening length and r_{200} . The corresponding M_{200} (in unit of $h^{-1}M_{\odot}$) and the concentration parameter c are listed in each panel.

firming the original result of Huss et al. (1999b). In Fig. 4, we present density profiles for 16 haloes with mass from $3 \times 10^{13} M_{\odot}/h$ to $4.5 \times 10^{15} M_{\odot}/h$. All these haloes include more than 10,000 particles. Here the concentration parameter is measured by fitting an NFW profile to the numerical results using logarithmically spaced radial bins in the range $2\epsilon < r < r_{200}$. The softening length ϵ and r_{200} are shown in the plot by vertical dotted lines. We find these profiles to follow the NFW model very well. It is also obvious that the ρ_s and c have a strong mass dependence. Both parameters increase with increasing halo mass. These mass dependences disagree with those in a CDM universe where more massive haloes have a lower ρ_s and c . In Fig. 5, we display the dependence of concentration parameter on halo mass for our two halo samples. In the lower panel, we present results for CDMRUN. The mass dependence, $c \propto M_{200}^{-0.12}$, is close to that found by Neto et al. (2007) and Macciò et al. (2007) $c \propto M_{200}^{-0.11}$. In the upper panel, we present this relation for HDMRUN. It is interesting that the mass dependence inverts and follows $c \propto M_{200}^{0.2}$: the more massive a halo, the larger its concentration parameter.

Many previous studies have found that the structural properties and the mass accretion histories of haloes are closely related in a CDM universe (e.g. Navarro et al. 1996, 1997; Wechsler et al. 2002; Zhao et al. 2003). Concentration increases with the formation time and the characteristic density ρ_s can be related with the mean cosmic density at the time of formation. In Fig. 6, we check this relation for our HDMRUN haloes. The formation time is defined here as the earliest time when half of the halo mass was in its main

progenitor. It is interesting that massive haloes form a bit earlier than their low mass counterparts in this cosmology. Combining with the $M_{200} \sim c$ relation showed in Fig. 5, we find that the earlier forming objects do indeed have a larger concentration parameter, in agreement with the result for a CDM universe. This indicates that here also the inner part is assembled during the fast early growth phase.

4.2 Kinematics

If haloes follow a universal density profile as discussed above, and are in an equilibrium state, then the solution of Jeans equation for spherical, isotropic systems indicates that their kinematic structure may also be universal. Taylor & Navarro (2001) have found that, for dark haloes in a CDM universe, there is a power-law relationship between “phase-space density” and radius: $\rho/\sigma^3 \approx r^{-\alpha}$ with $\alpha = 1.875$, where phase-space density is defined as the ratio of local matter density ρ to the cube of the local velocity dispersion σ . This phase-space density is inversely related to the local entropy density. In the semi-analytic extended secondary infall model, this nearly scale-free nature of ρ/σ^3 is a robust feature of virialized haloes in equilibrium (Austin et al. 2005). Further investigation of halo formation processes indicates that this scale-free feature cannot be the result of hierarchical merging; rather it must be an outcome of violent relaxation (Austin et al. 2005; Barnes et al. 2006). We show results for massive haloes in our HDM and CDM samples in Fig. 7. In order to reduce the noise, we stack the 20 most massive haloes in each case. Before the stacking,

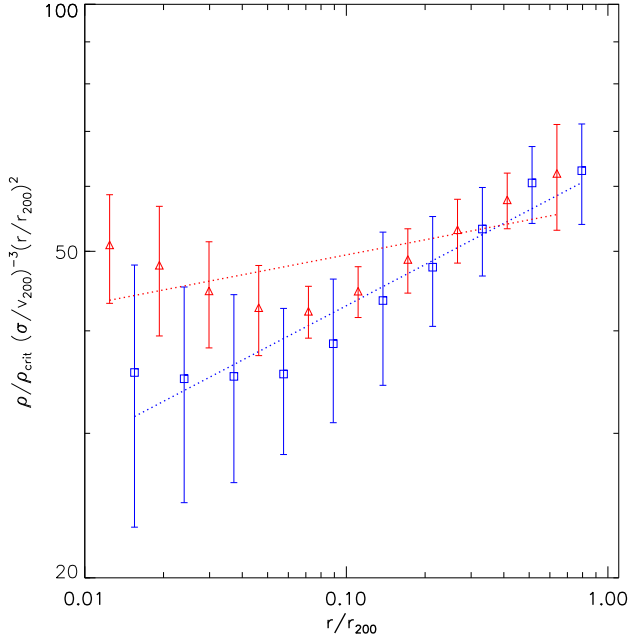


Figure 7. Stacked phase density profiles for the 20 most massive haloes in our two halo samples. The profile of each halo is normalized by a factor v_{200}^3/ρ_{crit} before stacking. The dotted straight lines are our power law fits with indices $\alpha = 1.94$ and $a = 1.83$ for HDMRUN (red triangles) and CDMRUN (blue squares) respectively. In order to get a better dynamic range, all symbols and lines multiplied by $(r/r_{200})^2$. The error-bars indicate the 1σ scatter.

the profile for each halo is normalized by a factor V_{200}^3/ρ_{crit} . The error-bars in the plot indicate the 1σ scatter. We find the two profiles to follow a power laws moderately well. The fitted indices differ slightly: $\alpha = 1.94$ and 1.83 for HDMRUN (red) and CDMRUN (blue) respectively.

In addition, the velocity anisotropy in haloes depends on radius: The dispersion tensor is isotropic near the center and moderately radially anisotropic near the virial radius. In Fig. 8, we present averaged velocity anisotropy profiles $\beta(r) = 1 - \sigma_t^2/\sigma_r^2$ for the 20 most massive haloes in our CDM and HDM samples. Here σ_t and σ_r are the tangential and radial velocity dispersions respectively. We again find very similar results for the two cases. Outside $0.2r_{200}$, the mean radial anisotropy in HDMRUN (red) is slightly larger than in CDMRUN (blue), but the effect is very small.

The similarities in phase-space density profile and velocity anisotropy profile in the two cases indicate that these properties are also universal and depend little on whether a halo is assembled by mergers or by monolithic collapse.

4.3 Halo Shape

In Fig. 9, we show axis ratios for haloes in HDMRUN and CDMRUN. We define the axes using the inertia tensor of the mass distribution within the virial radius r_{200} :

$$I_{\alpha\beta} = \frac{1}{N_p} \sum_{i=1}^{N_p} r_{i,\alpha} r_{i,\beta}. \quad (2)$$

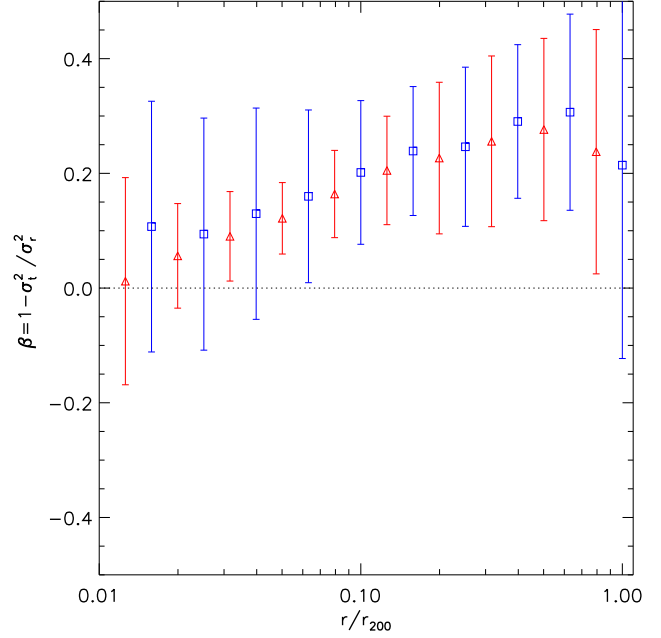


Figure 8. The stacked velocity anisotropy profile $\beta(r)$ for the 20 most massive haloes in the HDMRUN (red triangles) and CDMRUN (blue squares) samples. The error-bars indicate the 1σ scatter.

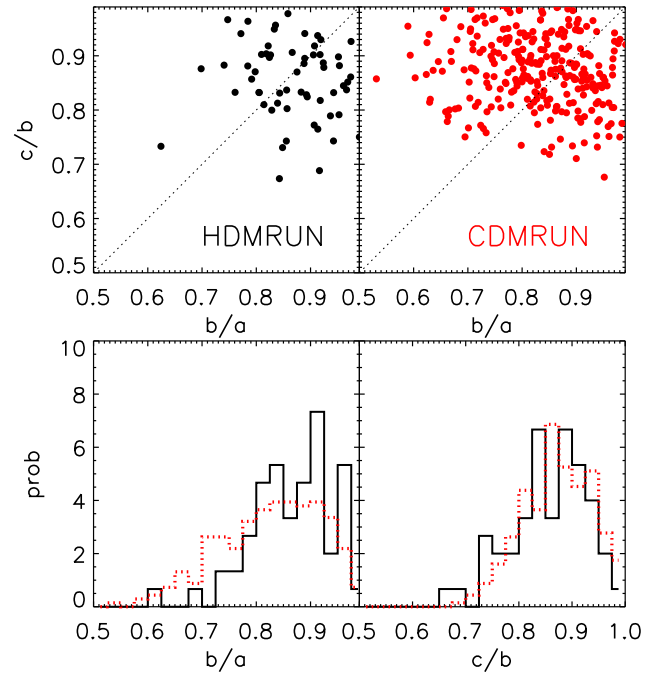


Figure 9. Scatter plots of the axis ratios of haloes in HDMRUN and CDMRUN (top two panels) and histograms of their probability distributions (lower two panels: red dotted and black solid curves are histograms for CDMRUN and HDMRUN respectively). Here a , b and c are the major, intermediate and minor axis lengths. Kolmogorov-Smirnov tests indicate that the distributions in two universes do not differ significantly.

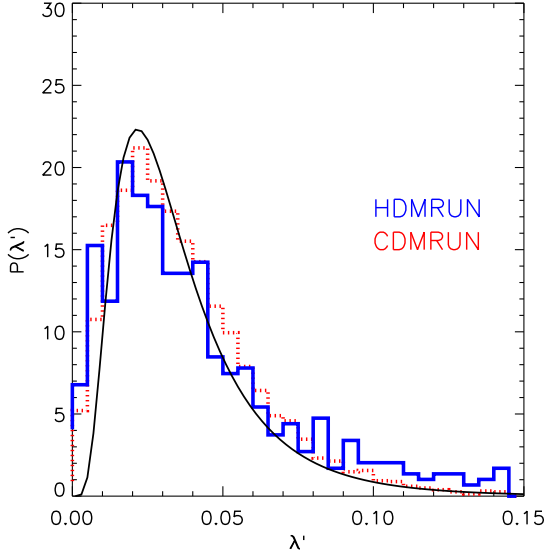


Figure 10. The probability distribution of the spin parameter λ' in HDMRUN (blue solid) and CDMRUN (red dotted). The black solid curve is the fit to a CDM universe from Bullock et al. (2001).

where the r_i are the positions of the N_p particles within r_{200} . α and β are tensor indexes with values of 1, 2 or 3 and indicate the three components of each particle's position. After diagonalizing this matrix, characteristic axis lengths are found as the square root of the eigenvalues. In the top two panels of Fig. 9, the intermediate-major (b/a) and minor-intermediate (c/b) axis ratios of halo samples from the two simulations are presented. The distributions of shape parameters are clearly very similar in the two cases. The mean values of the axis ratios b/a and c/b are both close to 0.82. In the lower two panels, we compare the probability distributions of b/a and c/b in the two simulations. The Kolmogorov-Smirnov test shows no evidence for any difference between the distributions in the HDM and CDM cases.

The above results indicate that different growth paths (monolithic or hierarchical) affect the global shape of halos very little.

4.4 Spin and Angular Momentum Distribution within Haloes

The conventional measure of halo angular momentum, the dimensionless spin parameter λ , is defined in terms of mass, energy and angular momentum and is related to the ratio between a halo's mean angular velocity (ω) and the angular velocity which would be required to support it by rotation alone (ω_0) (Peebles 1969):

$$\lambda \equiv \frac{J|E|^{1/2}}{GM^{5/2}} \simeq 0.4 \frac{\omega}{\omega_0}. \quad (3)$$

The total angular momentum J and energy E are needed to calculate this parameter. However, in this study, we follow Bullock et al. (2001) and define a more easily measured spin parameter λ' as:

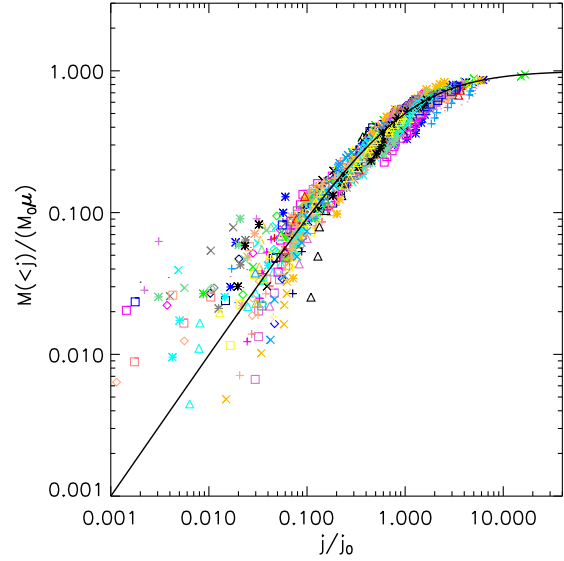


Figure 11. Mass distributions of specific angular momentum within 58 massive haloes in HDMRUN. Each coloured symbol presents one halo. Each mass distribution is normalized by its own virial mass (M_0) and shape parameter μ , all symbols then stay around the black curve $\frac{x}{1+x}$.

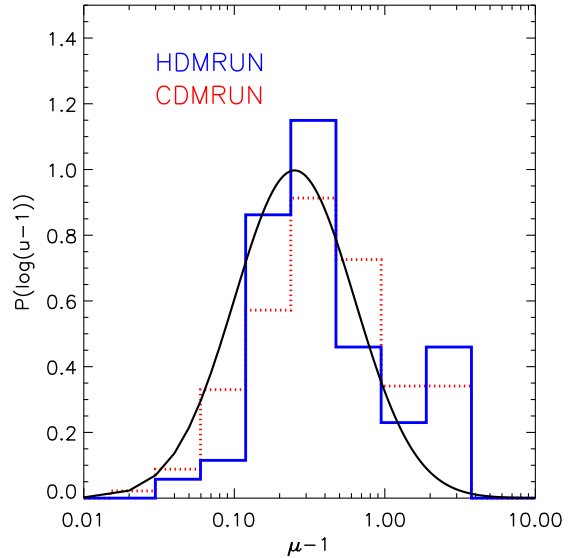


Figure 12. The probability distribution of the shape parameter μ in HDMRUN (blue solid) and CDMRUN (red dotted). The black solid curve is the fit to a CDM universe from Bullock et al. (2001).

$$\lambda' = \frac{J}{\sqrt{2}M_{200}Vr_{200}} \quad (4)$$

where J is the total angular momentum of all particles within r_{200} and $V = \sqrt{GM_{200}/r_{200}}$ is the circular velocity at radius r_{200} . This definition gives similar value to Equ. 3. Because λ' is defined for isolated systems but applied to haloes

in their cosmic context, the practical definition of a halo is more critical than the choice of definition of λ (Bett et al. 2007).

The net spin of a dark halo is acquired from torques exerted by neighbouring structures at early times (Hoyle 1949; Peebles 1969; Doroshkevich 1970; White 1984), and does not evolve much after the turnaround point of a halo’s MAH. After this time, the moment of inertia of the collapsing material decreases and the universal expansion reduces the strength of tidal forces (Porciani et al. 2002). Vitvitska et al. (2002) noted that the spin parameter fluctuates strongly with time, depending on the details of assembly: the spin increases abruptly during a major merger and decreases gradually between such mergers. D’Onghia & Navarro (2007) found this effect to reflect the unrelaxed nature of the system; equilibrium haloes show no significant correlation between spin and merging history. In our HDM simulation, most haloes grow in a monolithic way, so the impact from major mergers should be negligible.

In Fig. 10, we compare the distribution of spin parameters in our HDMRUN halo sample with that in the CDMRUN sample. A Kolmogorov-Smirnov test shows no significant difference between two different cases.

Bullock et al. (2001) noticed that the distribution of specific angular momentum j within the CDM haloes has a universal profile, specifically that the distribution of mass over specific angular momentum j is well fit in most haloes by the universal form:

$$M(< j) = M_0 \frac{\mu j}{j_0 + j} \quad (5)$$

where M_0 is the virial mass, which we here replace by M_{200} . $j_0 = (\mu - 1)j_{max}$ and j_{max} is the maximum specific angular momentum. This behaviour is not truly universal since μ is an adjustable shape parameter which varies from halo to halo. We now check this distribution for haloes in our HDM and CDM simulations.

In order to resolve the j profile adequately, we only consider haloes with particle number larger than 3×10^4 . Different regions are defined as cells in the usual spherical coordinates (r, θ, ϕ) . We make sure that each cell contains an approximately equal number of particles. We first divide the whole halo into 10 radial shells which host almost equal particle numbers. Then each shell is further divided into six zones: each cell spans the full 2π range in ϕ and spans the equal solid angle between $\cos(\theta) = -1$ and 1. The two zones with the same r and $|\cos(\theta)|$ that are above and below the equatorial plane are assigned to one cell. In Fig. 11, we present the distribution of normalized mass fraction $M(< j)/(M_0\mu)$ for 58 haloes from HDMRUN. Different coloured symbols present different haloes. We find that, after the parameter μ has been adjusted, all haloes are close to the curve $x/(1+x)$, thus the specific angular momentum profile can be described by one shape parameter μ very well. We compare the probability distribution of this parameter for the HDMRUN and CDMRUN samples in Fig. 12. The distributions are similar and close to a log-normal distribution as noted by Bullock et al. (2001) (A Kolmogorov-Smirnov test shows no indication of a difference.) A similar result was found by Chen & Jing (2002) for WDM haloes: the distribution is statistically indistinguishable from the CDM case. As in van den Bosch et al. (2002) and Chen & Jing (2002),

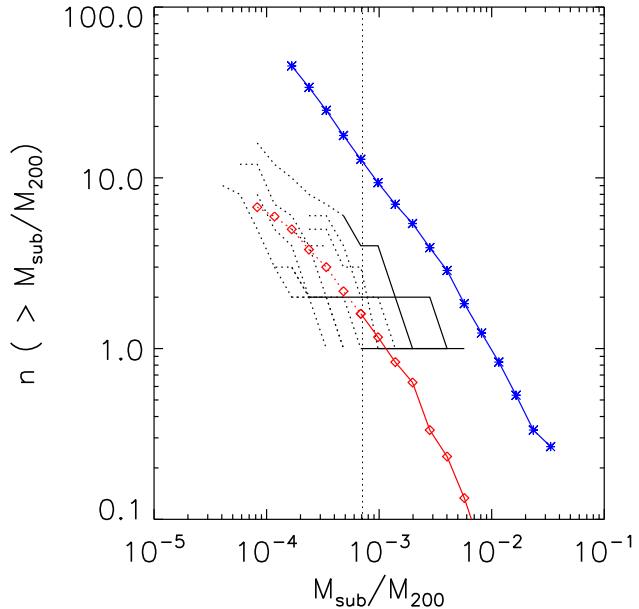


Figure 13. The stacked cumulative subhalo mass function of the 30 most massive haloes for our two samples: red diamonds and blue stars are for HDM and CDM haloes respectively. The results for several individual HDM haloes are also presented as black curves. The HDM curves are divided into two parts at $0.1M_{lim}$: real (spurious) subhaloes have masses greater (less) than this mass limit and are shown with solid (dotted) curves. The vertical dashed line indicates the mean mass limit for all 30 haloes in HDMRUN $< 0.1M_{lim} >$.

we also find some cells with negative angular momentum. These are excluded from our analysis.

The similarity between the distributions of spin parameter and internal specific angular momentum in the HDM and CDM cases shows that formation through mergers is not necessary to generate “universal” angular momentum distributions. This conflicts with the explanation which Vitvitska et al. (2002) give for the origin of the angular momentum distribution within CDM haloes.

4.5 Substructure

In Paper I, we gave a detailed discussion of the formation of substructures in a HDM Universe. We found almost all substructures in HDM haloes are either a result of spurious filament fragmentation (at low masses) or major mergers at late times (at large masses). As we see in Fig.1, at $z = 0.84$ and $z = 0.58$, there are many artificial regularly spaced objects falling into the clusters from filaments and these become substructures of the HDM haloes. This effect prevents us from studying the abundance of the real subhaloes at low mass since it is hard to identify which subhaloes (if any) are real. In Fig 13, we present cumulative mass functions of subhaloes for stacks of the 30 most massive haloes in each sample. For the HDM case, the subhalo mass functions of a few individual haloes are presented with black curves. For haloes in the HDM universe, we define ‘real’ subhaloes to

have mass greater than $0.1M_{\text{lim}} = 8.8 \times 10^{12} M_{\odot}/h$, and smaller subhaloes are considered ‘spurious’. The mass function of the ‘real’ and ‘spurious’ subhaloes are shown as solid and dotted lines respectively. The vertical dashed line indicates the mean mass limit $< 0.1M_{\text{lim}} >$ for all 30 haloes in the HDMRUN. We have assumed here that the average mass loss fraction is 0.1 when a subhalo falls into its parent halo and suffers tidal stripping. It is interesting that both distributions follow a similar power law. That of the HDMRUN sample is approximately one order of magnitude lower than the counterpart in CDMRUN and on average very few ‘real’ subhaloes are found in each halo in the HDM case. This reflects the lack of hierarchical build up in the HDM case.

5 CONCLUSIONS AND DISCUSSION

In this paper, we study the haloes which form by monolithic collapse in HDM cosmological simulations, and we compare a range of properties of these haloes with those of their counterparts in a Λ CDM hierarchical universe. From this comparison we explore which physical mechanisms are responsible for the universal profiles or distributions of halo properties. Our simulated HDM universe has an inherent characteristic scale below which the formation of small haloes is suppressed. In this universe, the first generation of halo forms in a “top-down” way – more massive haloes form earlier by smooth accretion. Mergers occur in significant numbers only when building up later halo generations. The HDM cosmology thus provides a good example of monolithic halo growth from Gaussian initial condition. Furthermore, because the HDM characteristic scale is much more sharply imprinted than in the WDM case, we have a large and well defined monolithic halo sample. As a result, we can explore monolithic growth in a better controlled way than previous work based on WDM universes. We summarise our conclusions on monolithic halo formation as follows:

(i) First generation haloes grow by smooth accretion. Such haloes form from roughly spherical collapse of matter around the nodes or ends of filaments. The formation histories of these monolithic haloes are also characterised by two phases: fast initial and slow later accretion, very similar to those found in a CDM universe. In the fast growth phase, smooth infall is the main mechanism rather than the mergers seen in the CDM case.

(ii) The density profiles of our monolithic haloes are well fit by the NFW profile. The concentration parameter c and the characteristic density ρ_s have strong dependences on halo mass: the more massive a halo, the larger c and ρ_s . This is the inverse of the CDM dependence, but the concentration-formation time relation is quite similar in the two cases: earlier formed haloes tend to be more concentrated than their later formed counterparts.

(iii) Phase-space density profiles and velocity dispersion anisotropy profiles are very similar in our two cases. This indicates that the kinematic structure of haloes is generated by wide variety of dynamical collapse processes, not just by mergers.

(iv) The distribution of shape parameter is very similar in HDM and CDM universes, as are the distributions of spin parameter λ' and of internal specific angular momentum.

(v) In our HDM simulations, most subhaloes result from the infall of spurious small haloes which form in the filaments as a result of numerical discreteness. The subhalo abundance is much lower than in CDM haloes, and indeed there are very likely no subhaloes in first generation HDM haloes.

The above results show that, except for substructure, the properties of haloes formed by monolithic collapse are very similar to those of haloes formed by hierarchical clustering in a CDM universe. In particular, they have very similar profiles of density, phase-space density and specific angular momentum, and very similar distributions of axial ratios and spin parameter. These results indicate that mergers are not responsible (or are not required) for the universal properties of CDM haloes. This agrees with results from earlier work based on constrained simulations (Huss et al. 1999a; MacMillan et al. 2006). Attempts to explain these universal properties with merger-driven models seem unlikely to be on the right track.

The results in this study could also find some applications in realistic dark matter models, especially for the WDM cosmology. In our HDM universe, first generation haloes form by smooth near-spherical accretion with initial mass well below the characteristic free-streaming mass. These haloes form simultaneously with the filaments and sheets. This picture is different from that in the familiar CDM universe. Our results suggest that the structure of the first haloes, in a WDM universe (and thus, presumably, also of their later descendants) will differ little from the structure of CDM haloes, despite the differences in assembly history. This makes it seem unlikely that changing to a WDM model will help resolve the apparent problems of the CDM model on galactic scales.

ACKNOWLEDGMENTS

We thank Volker Springel for providing us with the simulation code GADGET2 and with post-processing software. JW thanks Carlos Frenk for his hospitality at ICC, Durham where the draft of this paper was finished. JW also thanks Liang Gao and LiXin Li for useful comments. The simulations described in this paper were carried out on the Blade Centre cluster of the Computing Center of the Max-Planck-Society in Garching.

REFERENCES

- Allgood B., Flores R. A., Primack J. R., Kravtsov A. V., Wechsler R. H., Faltenbacher A., Bullock J. S., 2006, *MNRAS*, 367, 1781
- Austin C. G., Williams L. L. R., Barnes E. I., Babul A., Dalcanton J. J., 2005, *ApJ*, 634, 756
- Barnes E. I., Williams L. L. R., Babul A., Dalcanton J. J., 2006, *ApJ*, 643, 797
- Barnes J., Efstathiou G., 1987, *ApJ*, 319, 575
- Bertschinger E., 1985, *ApJS*, 58, 39
- Bett P., Eke V., Frenk C. S., Jenkins A., Helly J., Navarro J., 2007, *MNRAS*, 376, 215
- Bond J. R., Szalay A. S., 1983, *ApJ*, 274, 443
- Bullock J. S., 2002, in Natarajan P., ed., *The shapes of galaxies and their dark halos*, Proceedings of the Yale

- Cosmology Workshop , New Haven, Connecticut, USA, p.109 Shapes of dark matter halos. pp 109–+
- Bullock J. S., Dekel A., Kolatt T. S., Kravtsov A. V., Klypin A. A., Porciani C., Primack J. R., 2001, *ApJ*, 555, 240
- Bullock J. S., Kravtsov a. A. V., Colín P., 2002, *ApJ*, 564, L1
- Busha M. T., Evrard A. E., Adams F. C., 2007, *ApJ*, 665, 1
- Chen D. N., Jing Y. P., 2002, *MNRAS*, 336, 55
- Cole S., Lacey C., 1996, *MNRAS*, 281, 716
- Colín P., Avila-Reese V., Valenzuela O., 2000, *ApJ*, 542, 622
- Davis M., Efstathiou G., Frenk C. S., White S. D. M., 1985, *ApJ*, 292, 371
- Dekel A., Devor J., Hetzroni G., 2003, *MNRAS*, 341, 326
- Diemand J., Moore B., Stadel J., 2004, *MNRAS*, 353, 624
- D’Onghia E., Navarro J. F., 2007, *MNRAS*, 380, L58
- Doroshkevich A. G., 1970, *Astrophysics*, 6, 320
- Dubinski J., Carlberg R. G., 1991, *ApJ*, 378, 496
- Efstathiou G., Davis M., White S. D. M., Frenk C. S., 1985, *ApJS*, 57, 241
- Eke V. R., Navarro J. F., Steinmetz M., 2001, *ApJ*, 554, 114
- Fillmore J. A., Goldreich P., 1984, *ApJ*, 281, 1
- Gao L., Loeb A., Peebles P. J. E., White S. D. M., Jenkins A., 2004, *ApJ*, 614, 17
- Gao L., Navarro J. F., Cole S., Frenk C. S., White S. D. M., Springel V., Jenkins A., Neto A. F., 2008, *MNRAS*, 387, 536
- Gottlöber S., Turchaninov V., 2006, in Mamon G. A., Combes F., Deffayet C., Fort B., eds, *EAS Publications Series Vol. 20 of Engineering and Science, Halo Shape and its Relation to Environment*. pp 25–28
- Graham A. W., Merritt D., Moore B., Diemand J., Terzić B., 2006, *AJ*, 132, 2701
- Hahn O., Carollo C. M., Porciani C., Dekel A., 2007, *MNRAS*, 381, 41
- Hayashi E., White S. D. M., 2007, *ArXiv e-prints*, 709
- Hoyle F., 1949, *MNRAS*, 109, 365
- Huss A., Jain B., Steinmetz M., 1999a, *ApJ*, 517, 64
- Huss A., Jain B., Steinmetz M., 1999b, *MNRAS*, 308, 1011
- Kasun S. F., Evrard A. E., 2005, *ApJ*, 629, 781
- Macciò A. V., Dutton A. A., van den Bosch F. C., Moore B., Potter D., Stadel J., 2007, *MNRAS*, 378, 55
- MacMillan J. D., Widrow L. M., Henriksen R. N., 2006, *ApJ*, 653, 43
- Merritt D., Graham A. W., Moore B., Diemand J., Terzić B., 2006, *AJ*, 132, 2685
- Moore B., Ghigna S., Governato F., Lake G., Quinn T., Stadel J., Tozzi P., 1999, *ApJ*, 524, L19
- Navarro J. F., Frenk C. S., White S. D. M., 1996, *ApJ*, 462, 563
- Navarro J. F., Frenk C. S., White S. D. M., 1997, *ApJ*, 490, 493
- Neto A. F., Gao L., Bett P., Cole S., Navarro J. F., Frenk C. S., White S. D. M., Springel V., Jenkins A., 2007, *MNRAS*, 381, 1450
- Peebles P. J. E., 1969, *ApJ*, 155, 393
- Porciani C., Dekel A., Hoffman Y., 2002, *MNRAS*, 332, 325
- Power C., Navarro J. F., Jenkins A., Frenk C. S., White S. D. M., Springel V., Stadel J., Quinn T., 2003, *MNRAS*, 338, 14
- Ragone-Figueroa C., Plionis M., 2007, *MNRAS*, 377, 1785
- Raig A., González-Casado G., Salvador-Solé E., 1998, *ApJ*, 508, L129
- Salvador-Solé E., Solanes J. M., Manrique A., 1998, *ApJ*, 499, 542
- Springel V., White S. D. M., Jenkins A., Frenk C. S., Yoshida N., Gao L., Navarro J., Thacker R., Croton D., Helly J., Peacock J. A., Cole S., Thomas P., Couchman H., Evrard A., Colberg J., Pearce F., 2005, *Nature*, 435, 629
- Springel V., White S. D. M., Tormen G., Kauffmann G., 2001, *MNRAS*, 328, 726
- Subramanian K., Cen R., Ostriker J. P., 2000, *ApJ*, 538, 528
- Syer D., White S. D. M., 1998, *MNRAS*, 293, 337
- Taylor J. E., Navarro J. F., 2001, *ApJ*, 563, 483
- van den Bosch F. C., Abel T., Croft R. A. C., Hernquist L., White S. D. M., 2002, *ApJ*, 576, 21
- Vitvitska M., Klypin A. A., Kravtsov A. V., Wechsler R. H., Primack J. R., Bullock J. S., 2002, *ApJ*, 581, 799
- Wang J., De Lucia G., Kitzbichler M. G., White S. D. M., 2008, *MNRAS*, 384, 1301
- Wang J., White S. D. M., 2007, *MNRAS*, 380, 93 (Paper I)
- Warren M. S., Quinn P. J., Salmon J. K., Zurek W. H., 1992, *ApJ*, 399, 405
- Wechsler R. H., Bullock J. S., Primack J. R., Kravtsov A. V., Dekel A., 2002, *ApJ*, 568, 52
- White S. D. M., 1984, *ApJ*, 286, 38
- Zhao D. H., Mo H. J., Jing Y. P., Börner G., 2003, *MNRAS*, 339, 12

This paper has been typeset from a $\text{\TeX}/\text{\LaTeX}$ file prepared by the author.